

# Sizes of the Lightest Glueballs in $SU(3)$ Lattice Gauge Theory

Mushtaq Loan

*Department of Mechanics and Engineering, Zhongshan University, Guangzhou 510275, China  
School of Physics, The University of New South Wales, Sydney, NSW 2052, Australia*

Yi Ying

*Department of Physics, Chong Qing University, Chong Qing 400030, China*

(Dated: February 9, 2006)

Standard Monte Carlo simulations have been performed on improved lattices to determine the wave functions and the sizes of the scalar and tensor glueballs at four lattice spacings in the range  $a = 0.05 - 0.145$  fm. Systematic errors introduced by the discretization and the finite volume are studied. Our results in the continuum limit show that the tensor glueball is approximately two times as large as the scalar glueball.

PACS numbers:

## I. INTRODUCTION

Lattice calculations have yielded very accurate spectroscopic information regarding low-lying hadrons [1, 2] and glueballs [3, 4, 5, 6, 7, 8]. These calculations show that the lowest-lying scalar, tensor and axial vector glueballs lie in the mass region 1 - 2.5 GeV. While there is a long history of hadron and glueball mass calculations in lattice QCD, progress in determining their wave functions has not been so rapid. Although the spectrum of pure gauge QCD cannot be directly compared to experiment, it is important to pin it down because so little is known about glueball properties. The mixing of glueballs with  $q\bar{q}$  mesons due to the presence of light dynamical quarks makes it difficult in distinguishing them from ordinary mesons, both in full lattice QCD and in experiments [9]. Enormous effort have been made in pursuit of glueballs and their properties [10]. Accurate lattice calculations of their size, matrix elements and form factors would help considerably in the attempt to realize their experimental identification.

Glueball wave functions and sizes have been studied previously [11, 12, 13, 14], but much of the early works contain uncontrolled systematic errors, most notably from discretization effects. However, calculations using operator overlaps obtained from variational optimization for an improved lattice gauge action showed that the scalar and tensor glueballs are of typical hadronic dimensions. A straightforward procedure to determine glueball size is to compute measure the glueball wave function, much in the same way as in the meson and baryon wave functions were measured.

Although Ref. [11] produced interesting results, the approach used there suffers from a basic problem: The observables are calculated from lattice version of the 2-gluon operator, which risks the mixture of glueball states with the flux state<sup>1</sup>. Also the results are of limited inter-

est, because of their manifest dependence on the gauge chosen. In this study we take a more direct approach to the problem: Instead of fixing a gauge or a path for the gluons, we measure the correlation functions from spatially connected Wilson loops which, being the expectation values of closed-loop paths, are gauge invariant. The procedure has been used in the measurement of the wave functions of the scalar and tensor glueballs in the lattice Monte Carlo calculations in 3-dimensional  $U(1)$  theory [15]. This approach has the advantage that the detangling of the glueball and torelon is usually taken care of automatically by the choice of Wilson or Polyakov loops. This means that glueball operators cannot create a single torelon state, but the creation of torelon-antitorelon pairs is possible.

In this paper, we demonstrate the efficiency of our method in calculating  $SU(3)$  glueball wave functions using the tadpole-improved Symanzik action [6]. Since we want to explore the nature of the wave function, we focus on the sizes and masses of two of the lighter  $SU(3)$  glueball states, the scalar and the tensor. To avoid mixing effects, we adopt a quenched lattice QCD as a necessary first step before attempting to include the effect of dynamical quarks. It is worth mentioning here that quenched lattice QCD accurately predicts the important nonperturbative quantities as well as the masses of hadrons, mesons, and baryons. The remaining content of this paper are organized as follows. In Sec. II we give a prescription for calculating the glueball wave function and size based on the information from glueball correlators with the smearing method. We present and discuss our results in Sec. III. We close section with a comparison of our results with related QCD results. Concluding remarks are given in Sec. IV.

---

loops; some of these loops have a zero winding numbers and project onto glueballs others have non-zero winding numbers and project onto flux states, also called torelons.

---

<sup>1</sup> The link-link operator used there sums up a large number of

## II. WAVE FUNCTIONS OF GLUEBALLS

The lattice observables are computed as follows. First, we calculate the lattice operator

$$\Phi_i(\vec{r}, t) = \sum_{\mathbf{x}} [\phi_i(\vec{x}, t) + \phi_i(\vec{x} + \vec{r}, t)], \quad (1)$$

where  $\phi$  is the plaquette operator and  $\Phi$  is the two-plaquette or two-loop component of the glueball wave function. The summation over  $x$  is performed in order to obtain the zero-momentum projection. The  $r$  dependence is reflected in the length of the links required to close the loops.

Given a pair of orbit and spin quantum numbers  $L$  and  $S$  for the desired glueball, one can construct operators  $W(|\vec{r}|, t)$  with  $J = 0, 1, 2$ ,  $P = \pm$ , and  $C = \pm$  from suitable linear combinations of the rotation, parity inversions and real and imaginary parts of the operators involved in  $\Phi$ . In this study, we only consider  $S = L = 0$  (scalar  $0^{++}$ ) and  $S = 2, L = 0$  (tensor  $2^{++}$ ) glueball states. The two lattice observables measured are therefore

$$W_0(|\vec{r}|, t) = \sum_r [\Phi_{12} + \Phi_{13} + \Phi_{23}], \quad (2)$$

$$W_2(|\vec{r}|, t) = \sum_r [2\Phi_{12} - \Phi_{23} - \Phi_{13}]. \quad (3)$$

Using the glueball operators  $W$ , we consider the correlator

$$C(\vec{r}, t) = \langle W^\dagger(\vec{r}, t)W(\vec{r}, 0) \rangle, \quad (4)$$

where the vacuum expectation value must to be subtracted for the  $0^{++}$  glueball. The source can be held fixed, while the sink takes on the  $r$  dependence. This proves to be helpful in maintaining a good signal. In general, to measure the ground-state mass from the correlator, one seeks the region where the overlap with the lowest state is maximum and contributions from excited states are negligible. In principle, such a region always exists for large Euclidean time  $t$  in the zero-temperature case. However, in practice, it is difficult to use such large  $t$  in lattice QCD Monte Carlo calculations, since the correlator decreases exponentially with  $t$  and becomes so small for large  $t$  that it is comparable to its statistical errors. Hence, for the ground-state mass measurement, it is important that the ground-state overlap be sufficiently large. This leads to what amounts to a discrete search among wave functions. In the case of glueballs in quenched  $SU(3)$  lattice QCD, the overlap of the operators given in Eqs. (2) and (3) is quite small as long as they are constructed from the simple plaquette operators. This small overlap originates from the fact that the “size” of the plaquette operator is smaller (specifically of  $O(a)$ ) than the physical size of the glueball [16]. To improve the glueball operator, to enhance the ground-state contribution, we exploit the APE link smearing techniques

[16, 17] to generate extended operators with sizes that are approximately the same as the physical size of the glueball. The smearing procedure is implemented through the iterative replacement of the original spatial link variable by a smeared link. For the smearing parameters, which play an important role in extracting the ground-state contribution, we used a smearing fraction of  $\alpha = 0.5$  and a smearing number  $N_{\text{smr}} = 15$  in the present calculation. The optimum smearing is determined by examining the ratio

$$C(r, t+1)/C(r, t)$$

which should be close to unity for good ground state dominance. In fact, in the range  $4 \leq N_{\text{smr}} \leq 11$ , the above ratio is almost unchanged. For our measurements, with  $\alpha = 0.5$  fixed, a typical value that proved to be sufficient for most cases was  $N_{\text{smr}} = 4$  (although the results obtained with this value are almost the same as those with  $N_{\text{smr}} = 11$ ). For fixed  $\alpha$ ,  $N_{\text{smr}}$  plays the role of extending the size of the smeared operator and hence can give the rough estimate of the physical size of the glueball.

A second pass was made to compute the optimized correlation matrices

$$C_{ij}(t) = \langle W(r_i, t)W(r_j, 0) \rangle - \langle W(r_i) \rangle \langle W(r_j) \rangle. \quad (5)$$

Let  $\psi^{(k)}$  be the radial wave function of the  $k$ -th eigenstate of the transfer matrix. Then we have

$$C_{ij}(t) = \sum_k \alpha_k \psi^{(k)}(r_i) \psi^{(k)}(r_j) e^{-m_k t}. \quad (6)$$

The glueball masses and the wave functions are extracted from the Monte Carlo average of  $C_{ij}(t)$  by diagonalizing the correlation matrices  $C(t)$  for successive times  $t$ ,

$$C(t) = \tilde{R}(t)D(t)R(t), \quad (7)$$

where  $D$  is a diagonal matrix whose elements are eigenvalues and  $R$  is a rotation matrix whose columns are the eigenvectors of  $C$ . Each eigenvector of  $C$  corresponds to an eigenstate  $\psi^{(k)}(r)$  of the complete transfer matrix.

In order to investigate the size of the glueball, the Bethe-Salpeter amplitude provides a convenient tool. In the nonrelativistic limit, it is expected to reduce to the glueball wave function in the first-quantized picture. This property can be exploited to estimate the size of the glueball [11]. Similar to the case for mesons, the wave function is expected to decrease exponentially with the separation  $r$  and is therefore fitted with the simple form

$$\psi(r) \equiv e^{-r/r_0} \quad (8)$$

to determine the effective radius  $r_0$ .

The signal in the connected 2-point correlator  $C(t)$  for all observables does not last long to make to an exponential fit. For this reason, the data are presented in

terms of the effective mass read directly from the largest eigenvalue corresponding to the lowest energy,

$$m_{\text{eff}} = \log \left[ \frac{\lambda_0(r=0, t=1)}{\lambda_0(r=0, t=2)} \right]. \quad (9)$$

However, to ensure the validity of our results, we compared them to those obtained using

$$m'_{\text{eff}} = \left[ \frac{\lambda_0(t-1) - \lambda_0(t)}{\lambda_0(t) - \lambda_0(t+1)} \right]. \quad (10)$$

### III. SIMULATIONS RESULTS AND DISCUSSION

An ensemble of gauge configurations were generated using a combination of the Cabibbo-Marinari (CM) algorithm and the overrelaxed method. Configurations were given a hot start and then 100 compound sweeps (we define one compound sweep as one CM update followed by five over-relaxation sweeps) in order to equilibrate. After thermalization, configurations were stored every 50 compound sweeps for 750 configurations. Measurements made on the stored configurations were binned into 10 blocks with each block containing an average of 75 measurements. The mean and the final errors were obtained using the single-elimination jackknife method with each bin regarded as an independent data point. Four sets of measurements were taken to check the scaling of our results at  $\beta = 2.0, 2.25, 2.5$  and  $2.75$  on  $16^3 \times 16$  lattice. Some finite-size consistency checks were done on a  $12^3 \times 12$  lattice. Even though this lattice is relatively coarse, we can safely conclude that there are no large discretization errors after the implementation of the improved gauge and fermion actions.

The glueball correlation function for the  $0^{++}$  channel as a function of  $t$  at  $\beta = 2.5$  is shown in Fig. 1. The correlation function exhibits the expected exponential behaviour with respect to Euclidean time  $t$  for small values of  $r$ . Concerning the determination of the tensor glueball, we observe that the signal for the  $E^{++}$  channel is better than that for the  $T_2^{++}$  channel, and errors on the effective mass are reasonable. For this reason, we choose to use  $E$  of the tensor at finite lattice spacing. At  $\beta = 2.0$ , the signal does not persist long enough to demonstrate convergence to the asymptotic value; we present results for time separations  $t = 1$  and  $2$ . We found that Eqs. (9) and (10) yield consistent results in all cases analyzed here. The best estimates for the masses from our long runs are collected in Table I.

We extracted the wave functions at time-separations  $t = 1$ . Little difference between the eigenvectors of  $C(t)$  at  $t = 1$  and  $2$  was found. This suggests that there is no mixing between states of distinct masses. Typical plots of the wave functions, normalized to be unity at the origin, for the scalar and tensor glueballs at  $\beta = 2.25, 2.5$  and  $2.75$  are shown in Figs. 2 and 3, respectively. As a guide to the eye, Monte Carlo points corresponding to of the

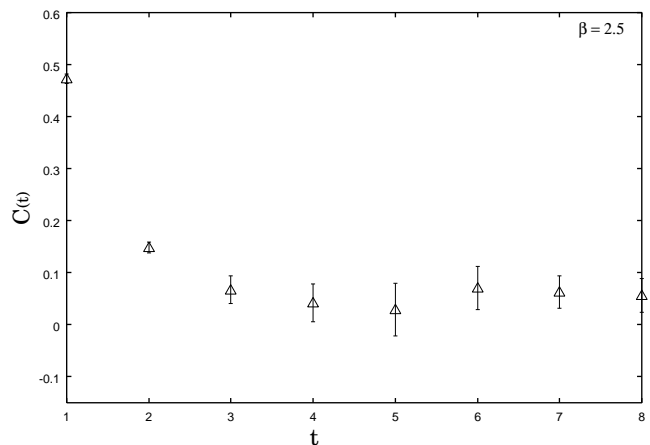


FIG. 1: Correlation function for the scalar glueball at  $\beta = 2.5$  on a  $16^4$  lattice

same value of  $\beta$  are connected with straight lines. The scalar wave function exhibits the expected behaviour and remains positive for all the values of  $\beta$  analyzed here.

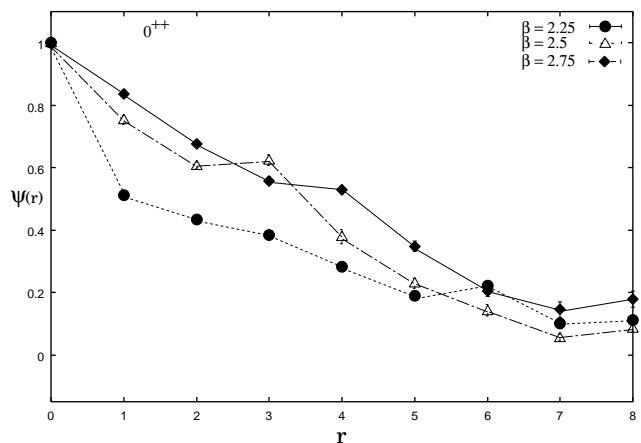


FIG. 2:  $SU(3)$  scalar glueball wave functions computed on a  $16^4$  lattice for various values of  $\beta$ .

We find that the tensor wave function shows the expected flatness and is much more extended than the scalar one as  $\beta$  increases. This would imply that tensor is more sensitive to finite-size effects, which is very visible in the distortion of the wave function for large  $r$  at  $\beta = 2.75$ . Naively, we expect that the spatial size at which we begin to encounter large finite-size effects is related to the size of the glueball. From optimization analysis at  $t = 1/0$ , we found that the  $4 \times 4$  and  $5 \times 5$  loops have better overlap with the glueball. This suggests that the glueballs have a size of  $\sim 4a - 5a$ . The smaller loops exhibit a weak signal and a slow convergence with  $N_{\text{smr}}$ . This is consistent with the findings of APE in the case that a  $1 \times 1$  loop is used as a template [16].

The size of the glueball is actually a nontrivial quantity. Although the charge radius of the glueball can be formally defined, its electric charges are carried by the

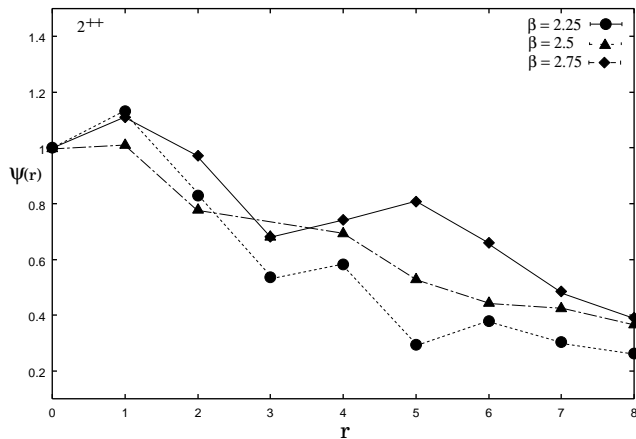


FIG. 3: Wave functions of the tensor glueball computed on a  $16^4$  lattice with  $\beta = 2.25, 2.5$  and  $2.75$ .

quarks and antiquarks, which play only secondary roles in describing the glueball state in the idealized limit, since the glueball does not contain any valence content of quarks (antiquarks). In principle, one could use Eq. (8) to extract the effective radius, but because of the distortion of the wave function at large  $r$  the results would depend strongly on the fit analysis of the above form. Even after the ground-state enhancement, the complete elimination of all the contributions of the excited states is impossible, especially near  $r \simeq 0$ . It follows that Eq. (8) holds only on a limited interval, which does not include the vicinity of  $r \simeq 0$ . Hence, for the accurate measurement of the effective radius, we need to find an appropriate fit range. To this end, we examine a plot of the effective-radius and the ratio

$$\log \left[ \frac{\psi(r)}{\psi(r+1)} \right]$$

for a given  $\psi(r)/\psi(r+1)$  at each fixed  $r$ . In Fig. 4 we plot the effective radius  $r_0$  as a function of  $r$  associated with Figs. 2 and 3 at  $\beta = 2.75$ . Figure 4 shows a non-trivial  $r$  dependence in the neighborhood of  $r \simeq 0$  in the effective radius of the tensor state. However, at large  $r$ , we see that there appears a region where  $r_0$  takes almost a constant value. Thus we conjecture that  $r_0$  consists of nearly a single spectral component, and hence can properly represent the effective radius. Estimates of the sizes, in lattice units, at various values of  $\beta$  values are listed in Table II.

In order to ascertain the finite-size effect on our measurements, we performed extra simulations for  $\beta = 2.5$  and  $2.75$ , using a lattice of spatial extent  $L = 12$ . The results from this spatial extension for glueball masses in terms of lattice units are given in Tables I and II, respectively. Note that the results for the smaller volume differ very little from those for  $16^3$  lattice, indicating that systematic errors in these results attributable to the finite volume are negligible. We also find that our estimates for the size of glueballs are consistent with the assump-

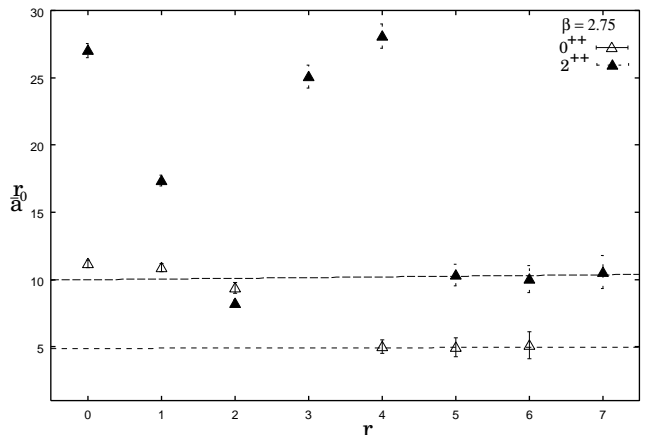


FIG. 4: The effective radius for the scalar and tensor glueball states at  $\beta = 2.75$ . The dashed horizontal lines indicate the plateau values.

tion that there is no large finite volume dependence at  $\beta = 2.75$ . Given that we use the larger lattice size to extract our results we can disregard any contamination of the glueball signal by a torelon-antitorelon pair, since no mass reduction of sufficient magnitude was found as the lattice volume was reduced (see Table I). This suggests that none of our states could be interpreted as a torelon pair.

TABLE I: Scalar and tensor glueball energy estimates in lattice units for the spatial extensions  $L = 12$  and  $L = 16$ . Also shown are our estimates of the rho mass at a physical point on the  $L = 16$  lattice.

$\beta/L$	Mass				
	$am_{0^{++}}$		$am_{2^{++}}$		$am_\rho(\kappa_c)$
	12	16	12	16	16
2.0		0.801(5)		1.42(2)	0.563(3)
2.25		0.58(1)		1.07(2)	0.391(4)
2.5	0.52(2)	0.527(3)	0.82(2)	0.824(16)	0.288(4)
2.75	0.43(2)	0.443(4)	0.64(2)	0.659(14)	0.227(4)

TABLE II: Effective radii of scalar and tensor glueballs in lattice units for the two spatial extensions  $L = 12$  and  $L = 16$ .

$\beta/L$	Size			
	$r_0^{0^{++}}/a$		$r_0^{2^{++}}/a$	
	12	16	12	16
2.0		1.37(7)		3.08(14)
2.25		2.9(1)		5.5(5)
2.5	4.1(1)	4.23(4)	7.6(8)	7.5(6)
2.75	4.8(2)	4.77(6)	10.0(1.3)	9.95(1.24)

To convert scalar and tensor glueball sizes and masses to physical units and extrapolate to the continuum limit,

we first need an estimate of the lattice spacing. One natural choice for this conversion factor is the rho mass,  $m_\rho a$ . Estimating the lattice spacing can be done by extrapolating the  $\rho$  mass to the physical quark mass<sup>2</sup>. Using a tadpole-improved clover fermion action we obtain the estimate  $1/\kappa_c = 6.362(3)$  by extrapolating the square pion masses from the largest five  $\kappa$  values at  $\beta = 2.5$ . We find that a linear fit of  $1/\kappa$  to  $m_\pi^2$  in  $1/\kappa$  works well for the rest of the coupling values analyzed here. Linearly extrapolating the  $\rho$  mass to  $\kappa_c$ , we find  $am_\rho(\kappa_c) = 0.288(4)$  or  $a^{-1} = 2.66(5)$  GeV, where the error is a jackknife estimate. The lattice spacings at other values of  $\beta$  are listed in Table III.

Another type of error that might effect the simulation results comes from the scaling violation for our action. Expecting that the dominant part of the scaling violation errors from the gauge and light quark sectors are largely eliminated by the tadpole improvement, we extrapolated the results obtained with finite  $a$  to the continuum limit,  $a \rightarrow 0$ . In practice, it is often difficult to quantify the magnitude of the systematic errors arising from this origin. Here, we adopt an  $a^2$ -linear extrapolation for the continuum limit, because the leading-order scaling violation is always  $O(a_s^2 \Lambda_{\text{QCD}} m_q)$ . We also performed an  $a$ -linear extrapolation to estimate systematic errors. We use the results obtained with the three finest lattice spacings for the continuum extrapolation, excluding the results obtained at  $\beta = 2.0$ , which appear to have large discretization errors as expected from the naive order estimate.

TABLE III: The lightest  $SU(3)$  glueball energy and size estimates in terms of the  $\rho$  mass.

$\beta$	$a(\text{fm})$	$m_{0^{++}}/m_\rho$	$m_{2^{++}}/m_\rho$	$r_0^{0^{++}} m_\rho$	$r_0^{2^{++}} m_\rho$
2.0	0.1444(6)	1.422(8)	2.53(4)	0.77(5)	1.73(4)
2.25	0.100(2)	1.50(2)	2.76(6)	1.15(4)	2.17(9)
2.5	0.073(3)	1.83(3)	2.86(4)	1.18(3)	2.2(1)
2.75	0.058(6)	1.95(4)	2.87(5)	1.12(5)	2.26(14)

Performing such extrapolations for mass and size we adopt the choice that yields the smoothest scaling behaviour for the final value, and use others to estimate the systematic errors.

Figure 5 displays our results for the scalar and tensor glueball radii in terms of  $m_\rho$ . It is seen that linear extrapolations in  $a^2$  yield better fits and the value in the continuum limit of  $1.14 \pm 0.08$  and  $2.27 \pm 0.03$  for the scalar and tensor states, respectively.

Note that the product  $r_0^{0,2} m_\rho$  varies only slightly over the fitting range. The three non-zero lattice spacing

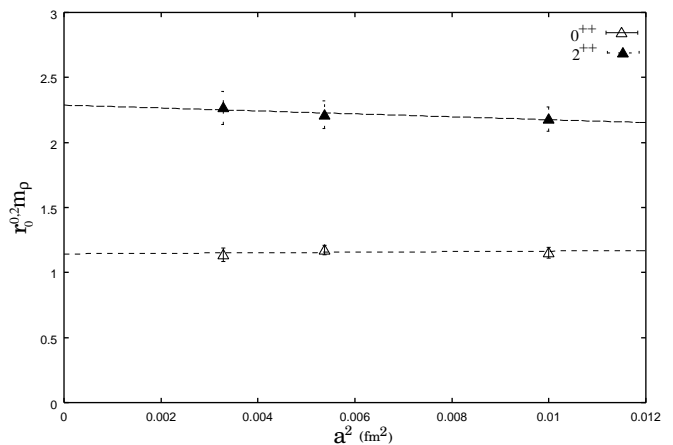


FIG. 5: Continuum limit extrapolation of glue radii in terms of  $\rho$  mass. The dashed curves are the best fits to the simulation results over the range  $0.0033 \leq a^2 \leq 0.01$ .

values of the product are within 0.02 - 0.04 and 0.01 - 0.09 standard deviations of the extrapolated zero lattice spacing result for the scalar and tensor state, respectively. This allows unambiguous and accurate continuum extrapolations. Figure 6 plots the dimensionless ratio  $m_{0,2}/m_\rho$  as a function of the square of the lattice spacing. Again, we expect a linear fit in  $a^2$  to provide the most reliable extrapolation to the  $a \rightarrow 0$  limit. Linear extrapolations to the continuum limit yield a scalar estimate of  $2.19 \pm 0.06$  and a tensor result of  $2.95 \pm 0.12$ . In contrast to the tensor, the scalar glueball mass shows significant finite-spacing errors. The continuum limit results obtained, in terms of the rho mass, are summarized in the Table IV.

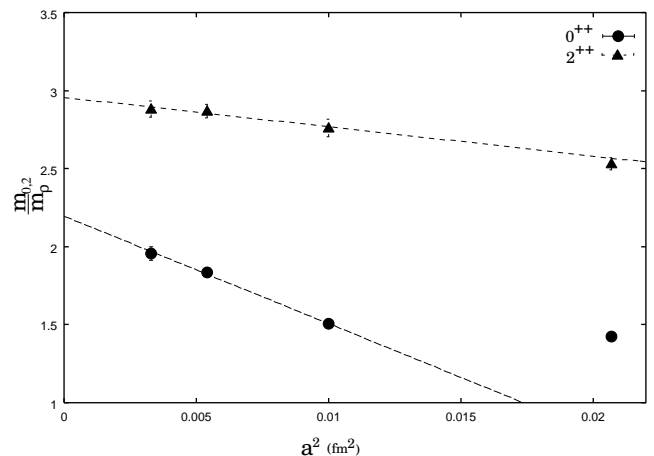


FIG. 6: Continuum limit extrapolation of the glue energy estimates in terms of the  $\rho$  mass. The curves represent linear fits to the data over the range  $0.0033 \leq a^2 \leq 0.01$ .

<sup>2</sup> Vaccarino and Weingarten [4] noted that extrapolating to zero lattice spacing using  $[\Lambda_{\overline{MS}}^{(N_f=0)}]^{-1}$  should give results nearly equivalent to those found using  $m_\rho(a)a$ .

To obtain the masses and the radii in units of MeV and fm, we used the experimental value 768 MeV for  $m_\rho$ . This yields radii of  $0.29 \pm 0.02$  and  $0.58 \pm 0.01$  fm for

TABLE IV: Continuum limit predictions for the scalar and tensor glueball masses and sizes and their conversion to MeV and fm, respectively.

$m_{0^{++}}/m_\rho$	$2.19 \pm 0.06$
$m_{2^{++}}/m_\rho$	$2.95 \pm 0.12$
$r_0^{0^{++}} m_\rho$	$1.14 \pm 0.08$
$r_0^{2^{++}} m_\rho$	$2.27 \pm 0.03$
$m_{0^{++}}$	$1680 \pm 46$ MeV
$m_{2^{++}}$	$2265 \pm 92$ MeV
$r_0^{0^{++}}$	$0.29 \pm 0.02$ fm
$r_0^{2^{++}}$	$0.58 \pm 0.007$ fm

the scalar and tensor glueballs, respectively. Our results show that the scalar glueball has a radius roughly equal to that of a pion [18], and the tensor glueball is about two times as large as the scalar glueball. We thus find that glueball size comparable in those of other hadrons. The continuum limit glueball mass results in MeV are summarized in Table IV. Our glueball mass results are in good agreement with those of previous calculations using the improved gauge action [3] as well as with those obtained with the Wilson action [4]. It is encouraging that the results are, within 10 – 15% errors, independent of the lattice action. We find that our glueball size estimates are consistent with the results reported in Ref. [14] obtained by using a Gaussian extension as the characteristic size of the glueball. We believe that our physical glueball sizes are more accurate than those obtained in Ref. [11] where it was found that the radius of the tensor glueball is three times that of a pion and four times that of a scalar glueball. The predicted zero lattice spacing results are in fact not found by extrapolation to zero lattice spacing, but are instead obtained from calculations with  $\beta = 2.2$  for the glueball effective radius. Assigning a physical value to the lattice spacing  $a$  by setting the string tension to 420 MeV, the physical radius is calculated with zero uncertainty, with no accurate representation of the effect of the absence of extrapolation.

#### IV. CONCLUSION

To conclude, we have calculated the  $SU(3)$  glueball wave functions using improved gauge and fermion lattice

actions. Instead of fixing a gauge or a path for gluons, the correlation functions were computed from gauge invariant closed-loop paths. This approach has an advantage over the method used in Ref [11], which can involve a mixing of the glueball states with torelons, and detangling of the glueball and torelon was done by hand. The iterative smearing procedure discussed here can be used to obtain a rough estimate of the physical glueball size in terms of a Gaussian extension. Although easy to implement, it does not give detailed information about the glueball wave function. A better approach may be to construct an elaborate smearing procedure that maps onto the wave function in one step (i.e., a variational method combined with fuzzing techniques).

Finally, we note that our results at the smallest lattice spacings seem to scale. This allows for very accurate extrapolations to the continuum limit. It is found that the physical size of the tensor glueball is about two times as large as that of the scalar glueball. This is consistent with the large finite-size effect for the tensor ( $E^{++}$ ) glueball mass found in previous lattice calculations. A great deal of care should be taken in making direct comparisons with experiment, since these values ignore the effects of light quarks and mixings with nearby conventional mesons. We intend to include the effect of dynamical quarks in a future study.

#### V. ACKNOWLEDGEMENTS

We thank D. Leinweber and C. Hamer for valuable conversations and suggestions. We are also grateful for access to the computing facilities of the Australian Centre for Advanced Computing and Communications (ac3) and the Australian Partnership for Advanced Computing (APAC). This work was supported by the Guangdong Provincial Ministry of Education.

- 
- |  |  |
|--|--|
| <p>[1] K. Bowler <i>et al.</i> (UKQCD Collaboration), Phys. Rev. D <b>62</b> (2000), 054506.</p> <p>[2] S. Aoki <i>et al.</i> (PC-PACS Collaboration), Phys. Rev. Lett <b>84</b> (2000), 238</p> <p>[3] C.J. Morningstar and M.J. Peardon, Phys. Rev. D <b>60</b> (1999), 034509; Phys. Rev. D <b>56</b> (1997), 4043.</p> <p>[4] A. Vaccarino and D. Weingarten, Phys. Rev. D <b>60</b> (1999), 114501.</p> | <p>[5] M. Teper, Phys. Lett. B <b>397</b> (1997), 223; Phys. Rev. D <b>59</b> (1998), 014512.</p> <p>[6] N.H. Shakespeare and H.D. Trotter, Phys. Rev. D <b>59</b> (1999), 014502.</p> <p>[7] G. Bali <i>et al.</i> (UKQCD Collaboration) Phys. Lett. B <b>309</b> (1993), 378.</p> <p>[8] G. Tickle and C. Michael, Nucl. Phys. B <b>333</b> (1990), 593.</p> <p>[9] J. Sexton, A. Vaccarino, and D. Weingarten, Phys. Rev.</p> |
|--|--|

- Lett. **75** (1995), 4563 and references therein.
- [10] K. Seth, Nucl. Phys. A **675** (2000), 25c and reference therein.
  - [11] P. de Forcrand and K-F Liu, Phys. Rev. Lett. **69** (1992), 245.
  - [12] T. DeGrand, Phys. Rev. D **36** (1987), 182.
  - [13] K. Ishikawa *et al.*, Nucl. Phys. B **227** (1983), 221.
  - [14] N. Ishii, H. Suganuma, and H. Matsufuru, Phys. Rev. D **66** (2002), 094506.
  - [15] M. Loan and Y. Ying, hep-lat/0603016 [e-print arXiv].
  - [16] M. Albanese *et al.*, Phys. Lett. B **192** (1987), 163
  - [17] T. Takahashi, H. Matsufuru, Y. Nemoto, and H. Sugaanuma, Phys. Rev. Lett. **86** (2001), 18
  - [18] B. Velikson and D. Weingarten, Nucl. Phys. B **249** (1985), 433